BMC Chemistry

RESEARCH Open Access

Synthesis, physicochemical, XRD/HSA-interactions, heteromeric [CH···Cl/CH···πPh] synthon, DFT, thermal and 1BNA-DNA molecular coupling of *cis*-Ni(S, N)$_2$ complex using hydrazine carbodithioate schiff base

Ahmed Boshaala[1*], Nawaf Al-Maharik[2], Hisham Qrareya[3], Abrahem F. Abrahem[1], Iman Muhmoud[1], Ibtisam Kaziri[4,5], Rabia Alghazeer[6], Nagi Greesh[1,7], Abdelkader Zarrouk[8], Khalil Shalalin[9] and Ismail Warad[10*]

Abstract

The reaction of bidentate-S, N-thione Schiff base ligand, Phenyl (E)-2-(1-phenylethylidene)-hydrazine-1-carbodithioate (PPEHCDT) with $NiCl_2.3H_2O$ produced a neutral $Ni^{II}(S, N)_2$ complex with cis form as kinetic favor isomer. Various physicochemical techniques, including EDX, FAB-MS, UV-Vis, IR, CHN, and XRD-crystal analysis, were employed to characterize the desired complex. These techniques provided evidence supporting the coordination of the ligand with the Ni-center, as indicated by the neutral *cis*-Ni(L)$_2$ formula. The XRD-results revealed a *cis*-isomer as anionic S-thiol and *bis*-bidentate-N-azomethine, as well as a slightly distorted square planar neutral *cis*-Ni(PPEHCDT)$_2$ complex. In contrast, the DFT simulation supported a distorted tetrahedral as favor geometry, despite the fact that the XRD/DFT structural parameters results agreed. Moreover, the Molecular Electrostatic Potential (MEP) together with the Hirshfeld Surface Analysis (HSA) confirmed the XRD seen in appearance of the Heteromeric sub-synthons *via* C-H$_{...}$.πPh and C-H···S interactions. Moreover, the TG/DTG technique exhibited a high level of stability (~ 250 °C) and a two-step thermal degradation process for the prepared *cis*-Ni(PPEHCDT)$_2$ complex. Furthermore, it has been observed that the molecular docking of 1BNA-DNA with the free ligand is superior to that of the *cis*-Ni(PPEHCDT)$_2$ complex due to the presence of two H-bonds with a larger binding energy as opposed to a single H-bond with a lower binding energy.

Keywords Ni(II) complex, DFT, Crystal structure, Hydrazonodithioate, HSA, Docking

*Correspondence:
Ahmed Boshaala
ahmedboshaala@yahoo.co.uk
Ismail Warad
warad@najah.edu

Full list of author information is available at the end of the article

Introduction

The transition metal ion nitrogen-sulfur bi-chelated ligand complexes that were accomplished from dithiocarbazic acid and S-alkyl thioesters were recently studied for their structural uniqueness and applications [1–4]. The mode of coordination of such ligands together with their thiol/thione isomerization pronounced their biological activities against cancer cells, viruses, microbes, fungal, and bacterial [2–4]. Moreover, the multifaceted industrial chemistry of ligand-complexes results in the participation of such new materials in non-biological and biological catalysis approaches [5]. Furthermore, the coordination of several types of hydrazonedithioate (as S and N ligands) is an essential piece of research to develop new complexes with industrial molecular magnetism, semiconducting behavior, electrochemical, and optoelectronic properties [6].

The transition metal ions $[M(S, N)_2]_n$ complexes using hydrazone dithioate ligands established several metal centers with different oxidation numbers of Fe(II&III), Mn(II, IV & VI), Co(III&II), Cu(I&II) and Ni(II), engage in the electrochemical oxidation of water [7–10]. $Ni(S, N)_2$ complexes were found to be the best catalysts among the others for the oxidation of water [11–16]. Therefore, the oxidation catalytic properties of such complexes, especially Ni(II) have been developed industrially for oxidation of enantioselective sulfides, alcohols, and alkenes [17–20]. In the natural biological system, Ni(II) with N, S containing bi-, tri-, or multi-chelated ligand complexes were used as a model for Ni(II)-enzymes like Ni-containing superoxide dismutase and bi-functional acetyl–CoA/carbon monoxide dehydrogenase synthase [21, 22].

In light of the growing interest in dithiocarbazic acid ligands and their metal complexes [1, 23–25], the primary objective of this study was to ascertain the molecular structure of the cis-Ni(PPEHCDT)2 complex during its interaction with the S-PPEHDC ligands. This study aimed to investigate the thiol-thione coordination mode behavior of the desired tridentate hydrazinecarbodithioate Schiff base via various physicochemical measurements, with particular emphasis on crystallographic XRD-one. The DFT, XRD, thermal behavior, HSA, MEP, MAC/NPA, DOS, HOMO/LUMO, and physicochemical properties together with their 1BNA-DNA docking behaviors were investigated.

Experimental

Chemicals and measurements

Chemicals and solvents fine are available from Fluka. In order to measure the infrared vibrations in the 4000–200 cm^{-1} wavenumber range, the PerkinElmer Spectrum 1000 FT-IR Spectrometer was used. The UV–Vis. data was achieved via TU-1901 double-beam spectrophotometer. Using a 711 A (8 kV) Finnigan, FAB-MS data were gathered. An Elementar Analyzer Varrio EL was used to get the CHN analysis.

Synthesis of Ni(II) complex

The PPEHCDT ligand and its Ni-complex were designed and synthesized in quantitative yield using a recent synthesis approach [1], based on our knowledge of hydrazinecarbodithioate polychelate ligands, which can act as tridentate or bidentate ligands, and insights from relevant literature reviews. It is noteworthy to notice that past publications have documented the utilization of distinct nickel transition components in the synthesis of analogous complexes [1, 23–25]. The desired complex was prepared by adding a hot solution of BPEHCDT ligand (0.31 g, 1.0 mmol) in 20 mL of ethanol to a solution of $NiCl_2.3H_2O$ (0.24 g, 1 mmol) in ethanol (30 mL). The mixture was stirred for an hour. The solution's volume was then reduced to half and refrigerated in a refrigerator for eight hours. The green precipitate was filtered and thoroughly washed with methanol and n-hexane, respectively. M.p 223 °C, yield in 76%. Anal. Calcd for $C_{30}H_{26}N_4NiS_4$: C, 57.24; H, 4.16; and N, 8.90. Found C, 57.21; H, 4.27; N, 8.73. FAB-MS: $[M^+] = 629.3$ m/z. Selected IR data (cm^{-1}): ν(C-H, Ph) 3080–3020 cm^{-1}, ν(C-H, alkyl) 2920–2890 cm^{-1}, ν(2 C = N) 1570 b, ν(N-N) 1118 s, ν(CSS) 825 cm^{-1}, v(Ni-N) 622 cm-^{1}, cm^{-1}, v(Ni-S) 502 cm-^{1}, cm^{-1}. UV–vis. Ligand bands like $\pi \rightarrow \pi^*$ at 238 nm, $\pi \rightarrow n$, at 302, $n \rightarrow \pi^*$ at 360, 397,238, 290, and d→d (Ni^{2+}) band at 420 nm.

Computation and XRD-crystal

HSA was achieved *via* CrystalExplorer platform, version 17 [26]. Gaussian W09 software was utilized for all the DFT stimulations [27]. The LANL2DZ was used as a basis set for Ni(II) the heavy atoms, while DFT 6-311G(d, p) was used for the other atoms. The docking studies were performed *via* Autodock 4.2 software, 2016 [28]. The 3D structure of the used DNA was obtained from the Protein Data Bank (PDB) via the 1bna code; the structure is readily accessible free on the PDB website [29]. The resolution of the 1BNA DNA structure, determined by SC-XRD, is 1.90 Å; the structure was obtained by crystallizing the protein under a precise method. The 1BNA-DNA structure is a distinguished B-form DNA dodecamer and was one of the first high-resolution DNA structures revealed using X-ray crystallography [30].

Single-crystal XRD data was collected on a Bruker AXS Smart Apex CCD diffractometer with graphite monochromatic Mo-K_α radiation of $\lambda = 0.071073$ Å at a temperature of 130 ± 2 K, using the scanning technique

to a maximum of 137 ± 2 K. The structure was solved by direct method employing SIR-92 and full-matrix least squares refinement [31]. All nonhydrogen atoms were anisotropically refined through SHELXL [32]. Hydrogen atoms were located geometrically and were refined isotropically. Table 1 reports the crystal data.

Results and discussion

Preparation, CHN-EA, MS, EDX and IR of cis-Ni(PPEHDC)$_2$ complex

To obtain the required *cis*-Ni(PPEHDC)$_2$ complex, the PPEHDC ligand was treated with $NiCl_2.3H_2O$ in a hot EtOH solution at room temperature, as shown in Scheme 1. The *cis*-Ni(PPEHDC)$_2$ complex was collected as a brownish powder with a good yield of 78%. The complex is slightly soluble in methanol, chlorinated solvents, and hot water but never in *n*-hexane. The *cis*-Ni(PPEHDC)$_2$ molecular structure was examined using various spectral techniques, including IR, FAB-MS, CHN-EA, UV-vis, EDX, TG/DTG, and XRD-crystal. The XRD result showed the PPEHDC ligand as S (thiol) and N (azometh) and not with thione form ligand mode of coordination.

Furthermore, it was observed that the cis-isomer of the neutral Ni(PPEHDC)$_2$ complex was exclusively obtained as the kinetically favored isomer. Conversely, there was no indication of the formation of the trans-Ni(PPEHDC)$_2$ complex isomer, which is thermodynamically favored. This observation has been substantiated through XRD-crystal analysis.

Cis-Ni(PPEHDC)$_2$ complex formula weight was confirmed by FAB-MS, $[M+1^+] = 629.3$ m/z (628.2 m/z theoretical). The CHN-elemental analysis aligns with the molecular formula of the complex $C_{30}H_{26}N_4NiS_4$. Moreover, EDX-analysis confirmed the purity and the atomic continent, as only energy peaks belong to C, N, S and Ni were detected, as shown in Fig. 1a.

The solid-state FT-IR of *cis*-Ni(PPEHDC)$_2$ complex was recorded, as seen in Fig. 1b. Several IR stretching vibration bands were observed; the main groups C_{Ph}-H, C_{alkyl}-H, C = N◊Ni, C = N, N-N, CS_2, N◊Ni and S◊Ni stretching vibrations were sited to 3080 – 3020, 2920 – 2890, 1575, 1570, 1118, 825, 622, 502 cm^{-1}, respectively. The same functional group stretching vibrations were observed by DFT-IR with slight shifts in their wavenumber values, as seen in Fig. 1c. Furthermore, the DFT and experimental IR wavenumber values exhibit a high level of agreement, as evidenced by a graphical correlation of 0.997, as seen in Fig. 1d.

Table 1 cis-Ni(PPEHCDT)$_2$ complex structure refinement data

Chemical formula	$C_{32}H_{30}N_4NiS_4$
CCDC	1503554
M_r	657.55
Crystal system, space group	Monoclinic, *C*2/*c*
Temperature (K)	130
a, *b*, *c* (Å)	24.715 (3), 8.4096 (9), 15.7655 (16)
β (°)	112.326 (2)
V (Å^3)	3031.1 (5)
Z	4
Radiation type	Mo *Kα*
μ (mm^{-1})	0.95
Crystal size (mm)	0.49 × 0.20 × 0.05
Diffractometer	Bruker AXS *SMART APEX*
Absorption correction	Multi-scan (*SADABS*; Sheldrick, 2004)
T_{min}, T_{max}	0.655, 0.954
No. of measured, independent and observed [$I > 2\sigma(I)$] reflections	13736, 3610, 3029
R_{int}	0.034
$(\sin\theta/\lambda)_{max}$ (Å^{-1})	0.658
$R[F^2 > 2\sigma(F^2)]$,	0.034,
$wR(F^2)$,	0.082,
S	1.06
No. of reflections, No. of parameters	3610, 187
$\Delta\rho_{max}$, $\Delta\rho_{min}$ (e Å^{-3})	0.48, −0.34

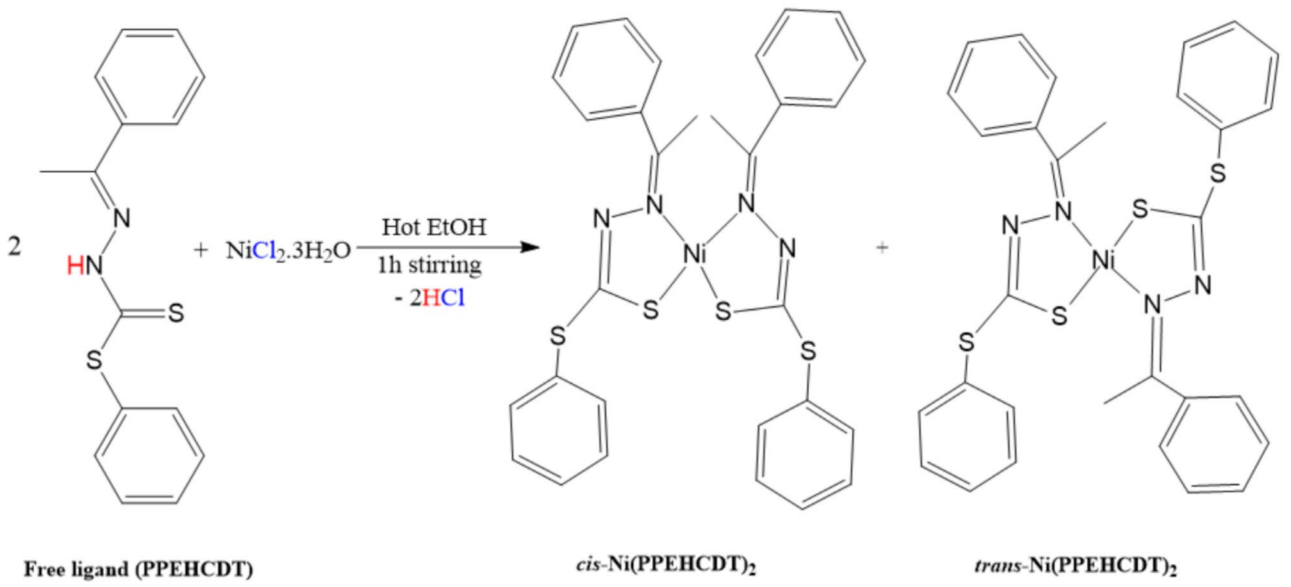

Scheme 1 *Cis*-Ni(PPEHDC)$_2$ complex synthesis

X-Ray and DFT computations

The DFT-optimized and ORTEP diagrams of *cis*-Ni(PPEHDC)$_2$ complex structures and their parameters have been illustrated in Fig. 2; Table 2. $C_{32}H_{30}N_4NiS_4$ is Monoclinic in crystal system, *C*2/*c* with Z = 4 per cell. The two PPEHDC ligands bonded to Ni(II) center *via* S and N provided by 2 anionic via S^- and 2 neutral N-groups to form the neutral *cis*-Ni(PPEHDC)$_2$ complex with two five-hetero-metal-membered center *cis*-Ni(N, S)$_2$ rings (Fig. 2b). The bond and angle values of the Ni(II)-complex are in high agreement with previously similar structures [1, 23, 24]. The Ni(II) center geometry was solved as a distorted square planar with τ = 30.2° (Fig. 2b). The DFT optimization result of the cis-Ni(PPEHDC)$_2$ complex revealed that the square planar geometry is more favourable than the tetrahedron geometry. This observation was not surprising since the DFT theory neglected any internal interactions (gaseous state). Hence, it is possible through DFT to observe that the tetrahedral structure around metal center is a preferred isomer over the square planar geometry because it has a lower steric hindrance that minimizes the internal repulsion. As the distorted square planar around the Ni(II) center has been confirmed experimentally by XRD-crystal, it can be said in this manuscript that the DFT-theory contradicted the results of XRD in judging the final geometry around the metal central atom, but it agreed in judging the other structural parameters.

The DFT-optimized angles and bond lengths were consistent with experimental XRD data, as shown in Fig. 3. Figure 3a shows acceptable levels of DFT and XRD in terms of angles and bond lengths. Bond lengths were in great agreement, as shown in Fig. 3a, with a graphical correlation R2 = 0.972 (Fig. 3b). Even two distinct geometries were proposed: the tetrahedral structure was seen by DFT and the square planar structure was validated by XRD; their angles also exhibited excellent agreement, as shown in Fig. 3c, with graphical correlation R2 = 0.9798 (Fig. 3d).

Heteromeric [CH···Cl/CH···πPh] synthon and HSA investigation

Typically, the occurrence of two primary large synthons of 2D-S24-type cyclic bonding is uncommon (Fig. 4a). This is because each synthon is composed of a triple-side sub-synthon, specifically 2S11 and 1S10, which bind through two short contacts: Calkyl-H…S with a radius of 2.902 μ and Cph-H…Ph with a radius of 2.974 γ (Fig. 4b). The non-classical shorter hydrogen bonds, specifically H…S and H…Ph, exhibit a two-dimensional chain formation, as depicted in Fig. 4b. Furthermore, the cis-Ni(PPEHDC)$_2$ lattice exhibited a notable increase in crystalline matrix stability as well as enhanced optical and electrical characteristics due to the presence of eight interactions per two synthons [33].

To confirm the packing result, the HSA of *cis*-Ni(PPEHDC)$_2$ was performed in between − 0.632 and 1.876 a.u. using the CIF crystallographic data [34–42]. The HSA and 2D-FP collected results are illustrated in Fig. 5. The existence of S and N heteroatoms together with π of the aromatic rings, in addition to several polar hydrogens, enhanced the formation of eight red-dots, including the presence of short interactions like H….S and H···πPh as seen in d_{orm} (Fig. 5a). Moreover,

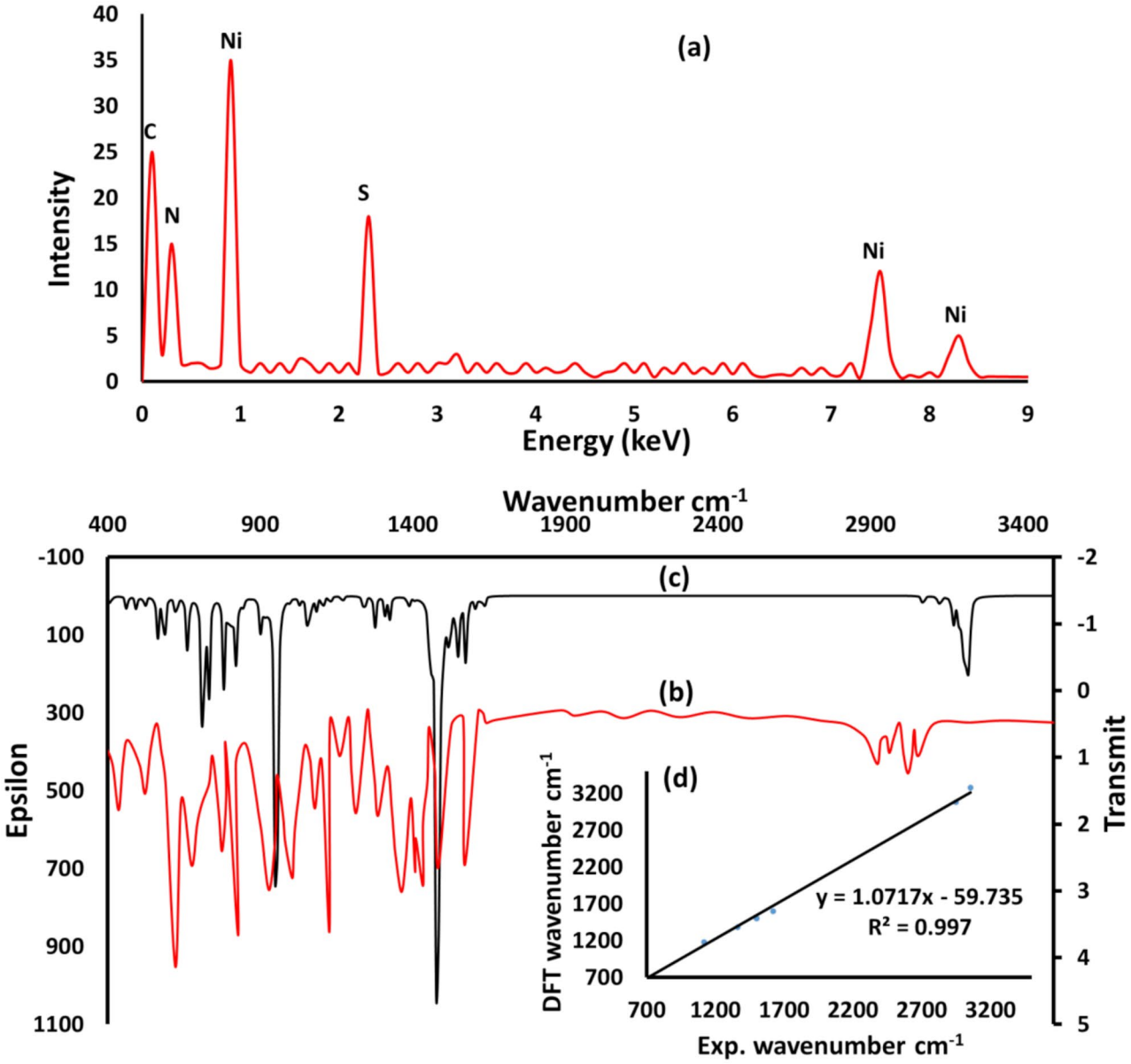

Fig. 1 (**a**) EDX spectra, (**b**) IR, (**c**) DFT and (**d**) DFT/Exp.-IR correlation diagram

2D-FP intermolecular H-to-atom ratios are displayed in Fig. 5b. It was found that the H···H (51.5%) interaction has the highest ratio among all interactions, while the H···Ni reflected a 0.1% ratio (Fig. 5c). The 2D-FP ratio analysis is illustrated in the following order: H….H > C….H > S…H> (N….H, Ni….H, 0%).

MEP, and MAC/NPA

MEP map of *cis*-Ni(PPEHDC)$_2$ complex is computed to explore the binding properties of the complex. The potential increased, ranging from blue, green, yellow, orange, and red, reflecting the degree of the electronic density of each atom. The MEP results indicated that the etheric S and coordinated S atoms display the highest e-rich/nucleophilic sites (red color). Meanwhile, the e-poor/electrophilic spots (blue) are highly seated on the phenyl and methyl protons. Usually, aromatic rings are rich with π electrons; they are distinguished as yellow areas (Fig. 6). Non-classical C-H···πPh and C-H···S H-bond interactions can be computed using MEP theory that is consistent with the HSA and XRD outcome. The atomic charge of our molecule surface behavior MAC and NPA charge distribution in *cis*-Ni(PPEHDC)$_2$ complex were calculated and displayed as seen in Fig. 6. In general, the NPA reflected the Ph charges with higher values compared to MAC results. All atomic charges of each atom on the surface of the core of the molecule were collected

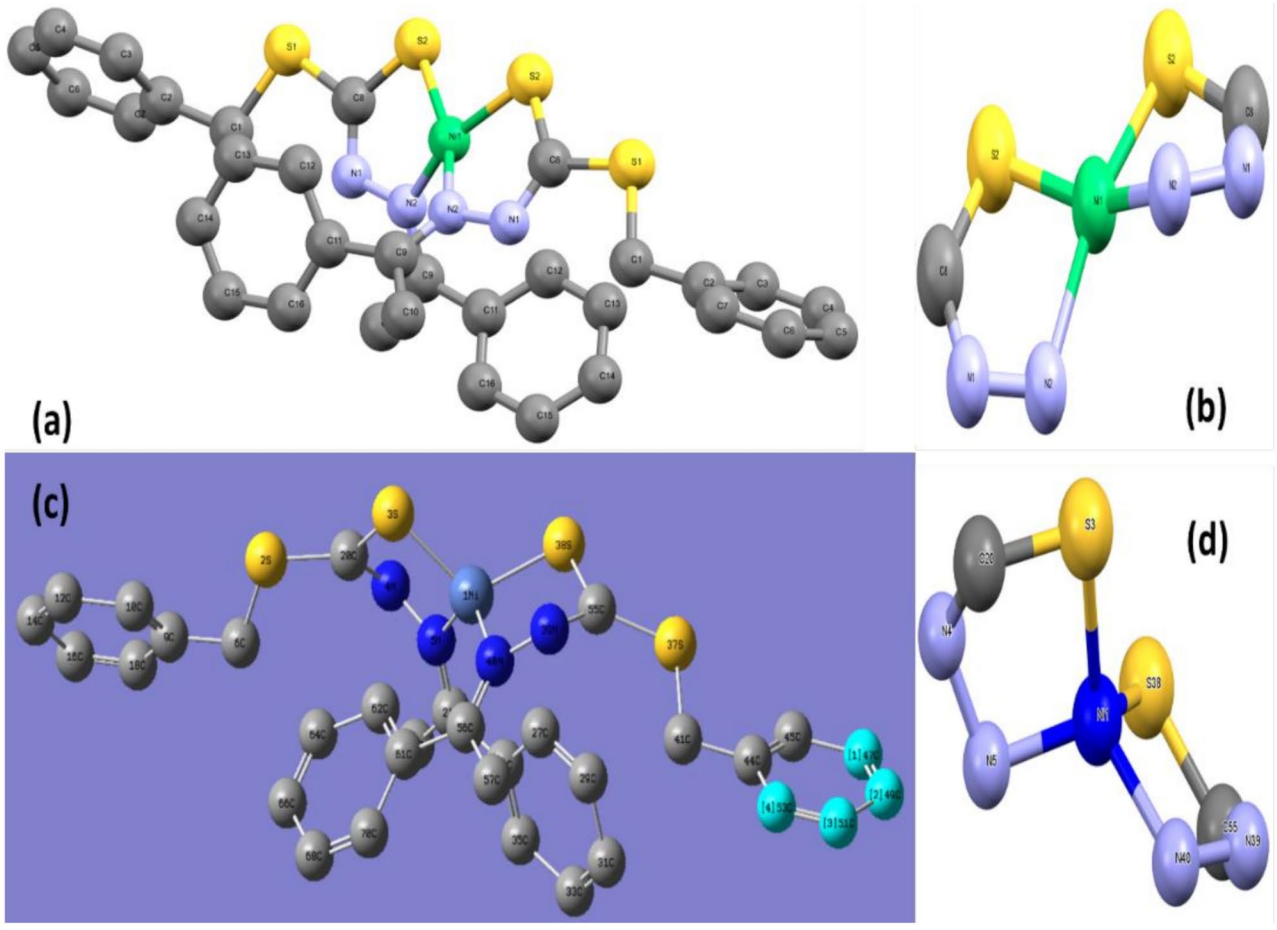

Fig. 2 (**a**) ORTEP diagram, (**b**) distorted square planar, (**c**) DFT optimization, and (**d**) DFT-tetrahedral structure of *cis*-Ni(PPEHDC)$_2$ complex

in Table 3. The comparative study of both the models, MAC and NPA, is accepted since a high graphical correlation is detected at 0.8921, as seen in Fig. 6d.

HOMO/LUMO and DOS

The HOMO and LUMO shapes and energy levels provide input about stability, the relationship orbitals, and the general chemical and structural properties of the prepared new compounds. In the HOMO, the main electron density focused around the Ni(II) and the core atoms of *cis*-Ni(PPEHDC)$_2$; meanwhile, in LUMO focus only around the core atoms and not on Ni(II) center. Both HOMO and LUMO defocused the terminal phenyls. Moreover, the $E_{LUMO,}$ E_{HOMO}, and ΔE were calculated to be -0.0833, -0.1921, and 0.1088 a.u (2.9598 eV), respectively, as shown in Fig. 7a. In order to verify the HOMO and LUMO energy values, they were calculated using another model, like the Density of State (DOS). The net energy resulted in by DOS ΔE_{DOS} was found to be consistent with $\Delta E_{HOMO/LUMO}$ with very close 2.988 eV, as seen in Fig. 7b.

TG/DTG analysis

The thermal behavior of the desired *cis*-Ni(PPEHDC)$_2$ complex has been performed in an ambient conditions using a heat rate of 10 °C/min via TG/DTG, as shown in Fig. 8. Figure 8 shows the complex exhibitin high thermal stability. The stability of the complex up to 250 °C can be attributed to the absence of uncoordinated or coordinated water molecules on the nickel atom. This is evidenced by the absence of any weight loss in the complex between 50 and 160 °C, as depicted in Fig. 8a. This finding is consistent with both the IR and XRD results. The desired complex underwent two primary decay processes. The initial step exhibited the most pronounced mass decay within the temperature range of 250–300 °C, with T_{DTG} = 280 °C (Fig. 8) and mass of 39.6%. This loss can be mainly attributed to the de-structured of one piece of the PPEHDC ligand to form *cis*-Ni(PPEHDC)$_2$ complex. Meanwhile, the second step involved a wide range of temperatures from 420 to 510 °C, with T_{DTG} = 480 °C and mass loss of 40.5%.This loss can be attributed to the de-structuring of the second ligand component, which occurred

Table 2 Designated DFT/XRD bonds and angles lengths

Bond No.	Bond type		Bond length [Å]		Angle No.	Angle type			Angle value (°)	
			XRD	DFT					XRD	DFT
1	Ni1	S2	2.1759	2.2912	1	S2	Ni1	N2	86.02	89.35
2	Ni1	N2	1.906	1.7947	2	S2	Ni1	S2	98.44	97.78
3	Ni1	S2	2.1759	2.2911	3	S2	Ni1	N2	159.84	151.42
4	Ni1	N2	1.906	1.7947	4	N2	Ni1	S2	159.84	151.43
5	S1	C1	1.830(2)	1.9333	5	N2	Ni1	N2	96.56	97.52
6	S1	C8	1.747(2)	1.8185	6	S2	Ni1	N2	86.02	89.35
7	S2	C8	1.756(2)	1.7961	7	C1	S1	C8	100.7(9)	99.66
8	N1	N2	1.408(2)	1.4633	8	Ni1	S2	C8	92.33	88.7
9	N1	C8	1.292(2)	1.2988	9	N2	N1	C8	110.5(1)	111.7
10	N2	C9	1.300(2)	1.313	10	Ni1	N2	N1	118.2	119.34
11	C1	C2	1.502(2)	1.5018	11	Ni1	N2	C9	127.2	128.37
12	C2	C3	1.389(3)	1.402	12	N1	N2	C9	114.6(1)	112.27
13	C2	C7	1.390(3)	1.4019	13	S1	C1	C2	110.3(1)	108
14	C3	C4	1.381(3)	1.3949	14	C1	C2	C3	120.7(2)	120.45
15	C4	C5	1.379(4)	1.3973	15	C1	C2	C7	120.3(2)	120.6
16	C5	C6	1.377(4)	1.397	16	C3	C2	C7	119.0(2)	118.95
17	C6	C7	1.391(3)	1.3953	17	C2	C3	C4	120.6(2)	120.59
18	C9	C10	1.497(3)	1.5078	18	C3	C4	C5	120.0(2)	120.06
19	C9	C11	1.483(2)	1.4743	19	C4	C5	C6	120.3(2)	119.77
20	C11	C12	1.393(2)	1.4055	20	C5	C6	C7	120.0(2)	120.1
21	C11	C16	1.394(2)	1.4076	21	C2	C7	C6	120.2(2)	120.54
22	C12	C13	1.388(2)	1.394	22	S1	C8	S2	116.1(1)	116.04
23	C13	C14	1.387(3)	1.3961	23	S1	C8	N1	119.0(1)	118.08
24	C14	C15	1.382(3)	1.3998	24	S2	C8	N1	124.8(1)	125.89
25	C15	C16	1.385(3)	1.393	25	N2	C9	C10	122.3(2)	120.73
26	S1	C1	1.830(2)	1.9333	26	N2	C9	C11	118.8(2)	119.94
27	S1	C8	1.747(2)	1.8186	27	C10	C9	C11	118.9(2)	119.2
28	S2	C8	1.756(2)	1.7961	28	C9	C11	C12	119.9(2)	119.83
29	N1	N2	1.408(2)	1.4633	29	C9	C11	C16	120.6(2)	121.09
30	N1	C8	1.292(2)	1.2987	30	C12	C11	C16	119.4(2)	119
31	N2	C9	1.300(2)	1.313	31	C11	C12	C13	120.1(2)	120.51
32	C1	C2	1.502(2)	1.5019	32	C12	C13	C14	120.1(2)	120.1
33	C2	C3	1.389(3)	1.402	33	C13	C14	C15	120.0(2)	119.87
34	C2	C7	1.390(3)	1.4019	34	C14	C15	C16	120.4(2)	120.2
35	C3	C4	1.381(3)	1.3949	35	C11	C16	C15	120.1(2)	120.31
36	C4	C5	1.379(4)	1.3972	36	C1	S1	C8	100.7(9)	99.66
37	C5	C6	1.377(4)	1.397	37	N2	N1	C8	110.5(1)	111.7
38	C6	C7	1.391(3)	1.3954	38	N1	N2	C9	114.6(1)	112.27
39	C9	C10	1.497(3)	1.5079	39	S1	C1	C2	110.3(1)	108
40	C9	C11	1.483(2)	1.4743	40	C1	C2	C3	120.7(2)	120.45
41	C11	C12	1.393(2)	1.4055	41	C1	C2	C7	120.3(2)	120.6
42	C11	C16	1.394(2)	1.4076	42	C3	C2	C7	119.0(2)	118.95
43	C12	C13	1.388(2)	1.394	43	C2	C3	C4	120.6(2)	120.58
44	C13	C14	1.387(3)	1.3961	44	C3	C4	C5	120.0(2)	120.06
45	C14	C15	1.382(3)	1.3998	45	C4	C5	C6	120.3(2)	119.77
46	C15	C16	1.385(3)	1.393	46	C5	C6	C7	120.0(2)	120.1

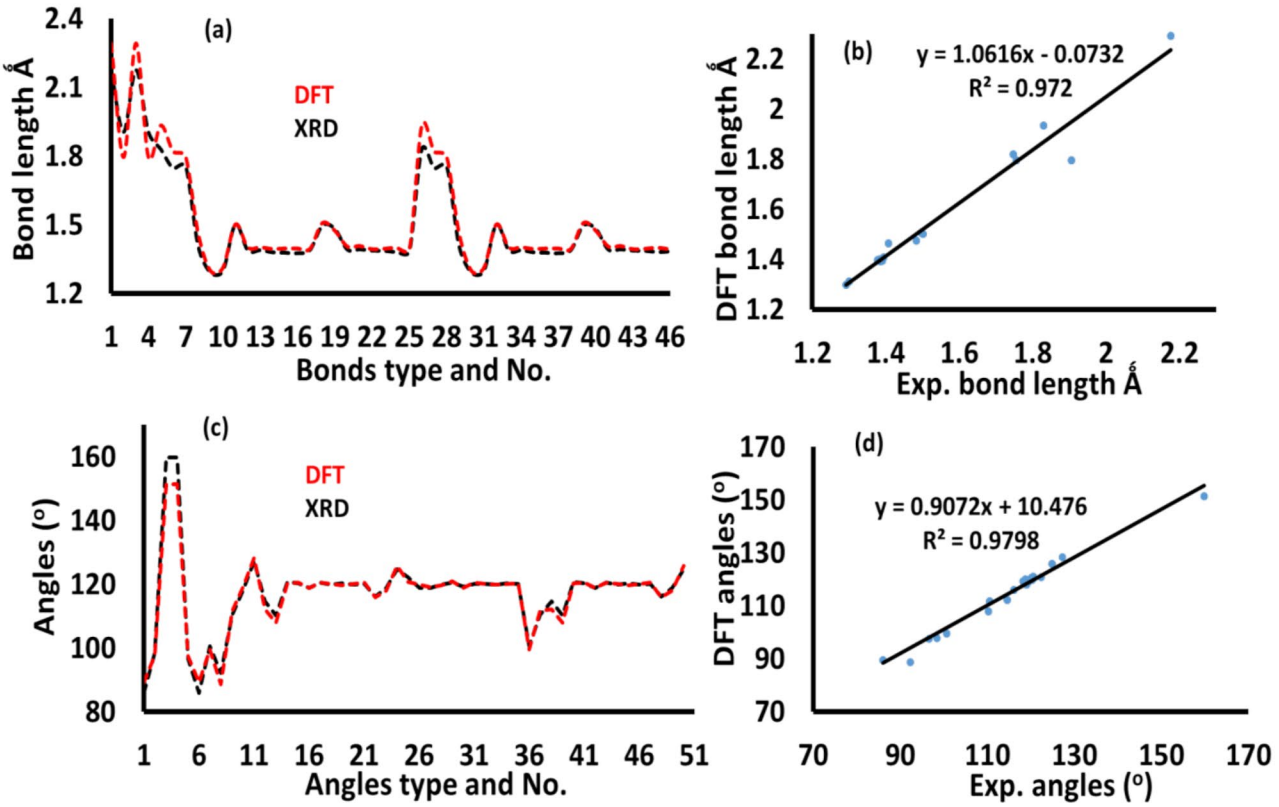

Fig. 3 (**a**) XRD/DFT-bond lengths histogram, (**b**) XRD/DFT-bond lengths graphical correlation, (**c**) XRD/DFT-angles histogram, and (**d**) DFT/Exp. angles correlation diagram

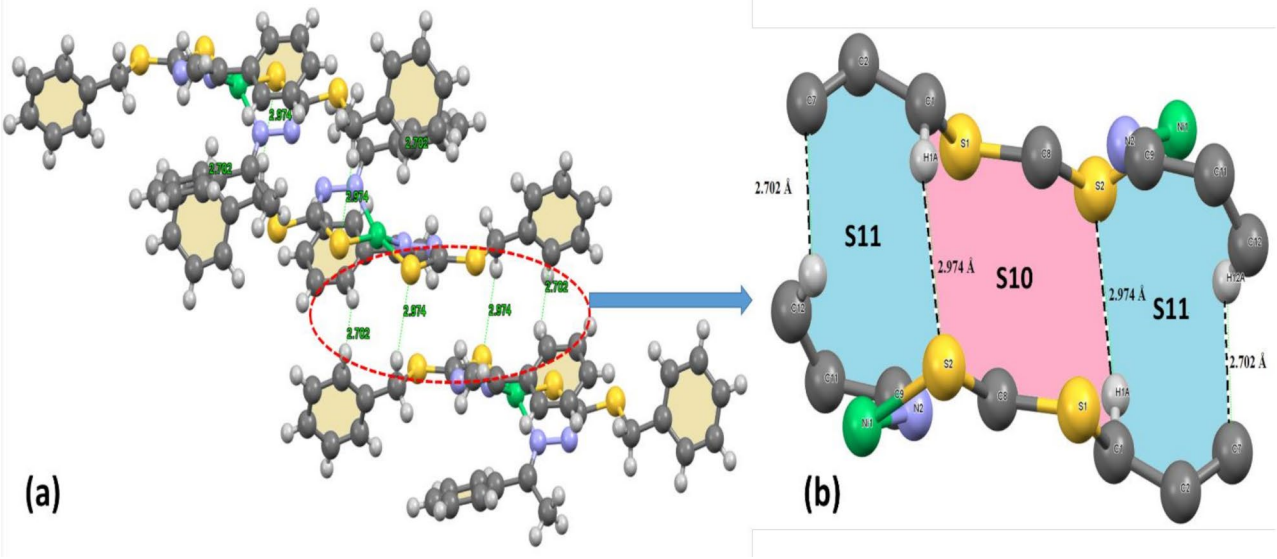

Fig. 4 (**a**) 2D-S24 triple sub-synthon, and (**b**) 2S11 + S10 sub-synthons including H….S and H···πPh interactions

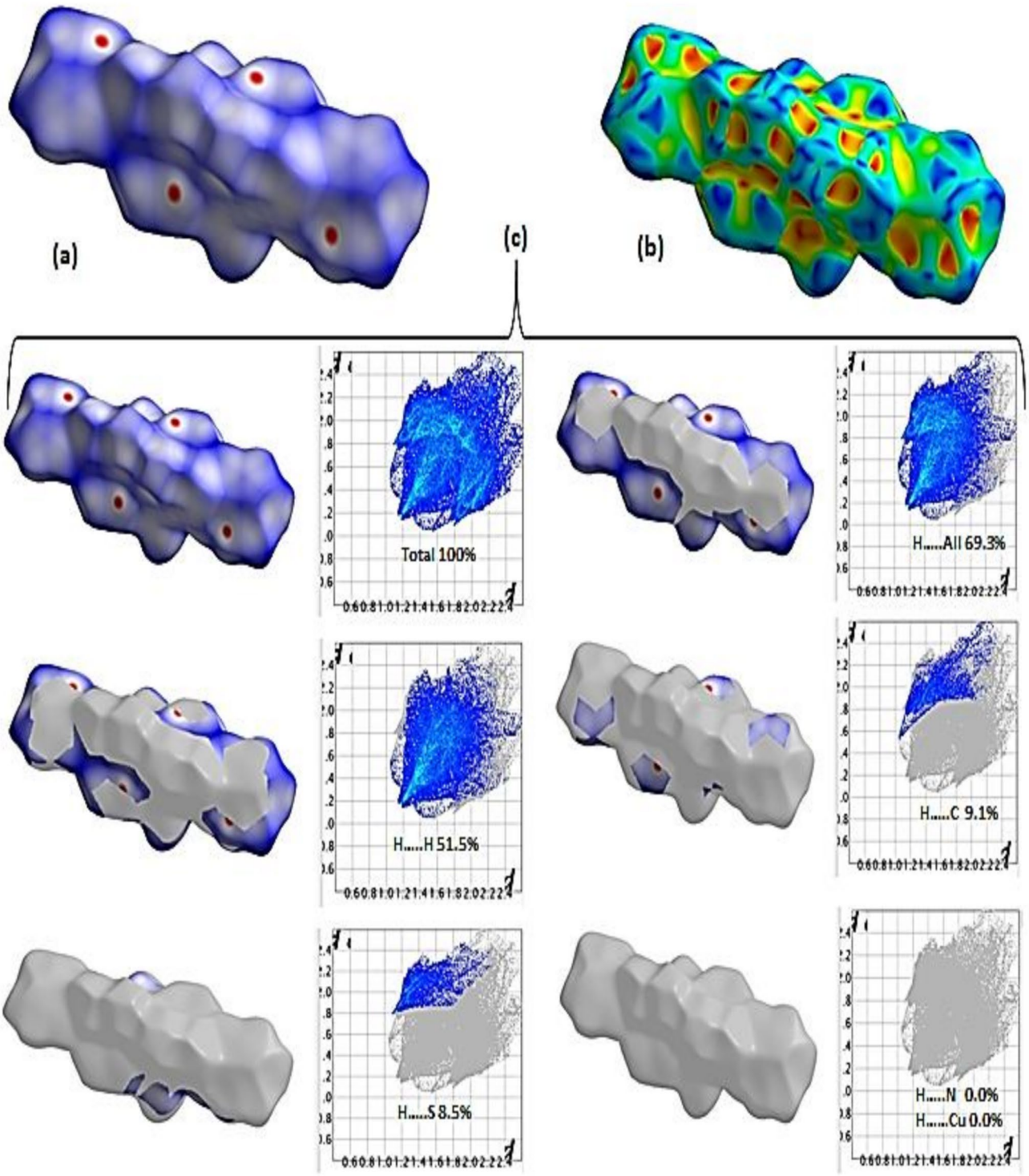

Fig. 5 (**a**) d_{norm}, (**b**) shape index, and (**c**) 2D-FP over the *cis*-Ni(PPEHDC)$_2$ complex surface

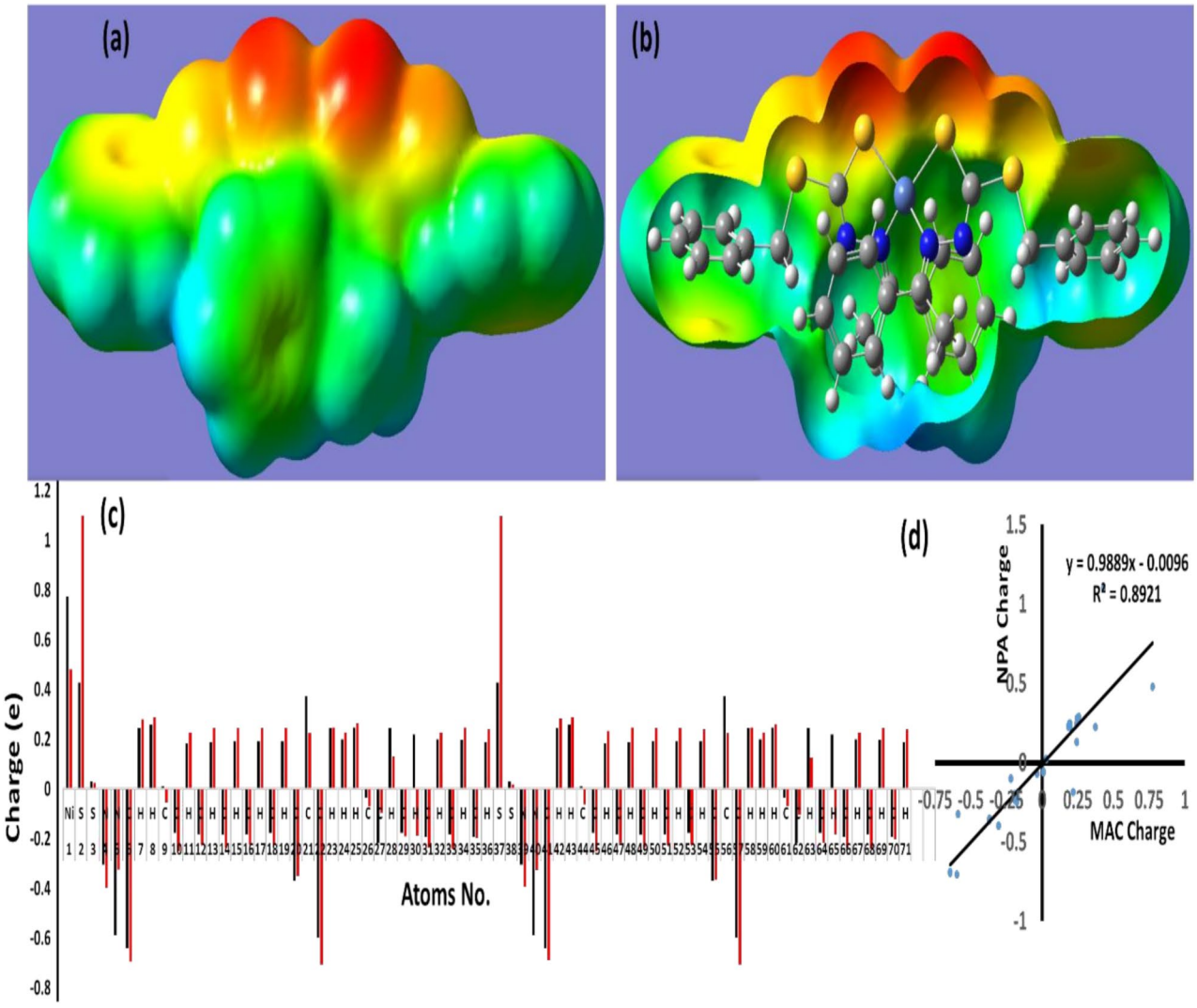

Fig. 6 (**a**) MEP, (**b**) MAC/NPA, (**c**) MAC vs. NPA, and (**d**) MAC/NPA correlation of *cis*-Ni(PPEHDC)$_2$ complex

simultaneously with the reaction with atmospheric O_2 to produce nickel oxide as a final product with ~ 19.3% yield [44].

Molecular docking studies

In the field of structural drug design (SDD), understanding the binding of medications to DNA or enzymes can be accomplished by the most successful theoretical molecular coupling method, which distinguished as an outstanding methodology [43–45]. The methodology in this section focuses on the interaction between the free PPEHCDT ligand and its *cis*-Ni(PPEHCDT)$_2$ complex with 1BNA-DNA helices. This algorithm will analyze different positions, orientations, and types of interaction between PPEHCDT or cis-Ni(PPEHCDT)$_2$ and DNA using Autodock 4.2 [28] output virtualized via PyMOL [46] software. Its goal is to identify the configuration that offers the greatest fit to assess the experimental better future chemotherapy. Table 4; Fig. 9 show the final docked pictures and the binding energy estimates for the ligand and its complexes. The PPEHCDT docked with 1BNA resulted like the cisplatin binding mode; mimic a good docking by cross-linking of the 1BNA both double helix [42] with a minor grove site interaction (Fig. 9a) via two short hydrogen bonds. The first was via NH of hydrazine carbodithioate and cytosine (DC23:O4) bases of DNA with 1.985 Å length, and the second hydrogen bond was through sulfur of dithioate and guanine (DG4:H22) bases of DNA with 2.323 Å length (Fig. 9b). These two H-bond result the binding energy with a very good value of -8.84 kcal/mol. Other weak binding interactions as Ph π: π, S-π and VdW, were also recorded, as seen in Fig. 9b. A dramatical change in the bonding mode was obtained when the *cis*-Ni(PPEHCDT)$_2$ was introduced instead of the

Table 3 NPA/MAC charge population

No.	Atom	MAC	NPA	No.	Atom	MAC	NPA
1	Ni	0.773991	0.47953	37	S	0.428473	1.09673
2	S	0.428479	1.09846	38	S	0.029384	0.01851
3	S	0.029393	0.02495	39	N	-0.30618	-0.39583
4	N	-0.30617	-0.39799	40	N	-0.58893	-0.32677
5	N	-0.58894	-0.32517	41	C	-0.6439	-0.68963
6	C	-0.6439	-0.69496	42	H	0.245213	0.2827
7	H	0.245211	0.27978	43	H	0.257552	0.28873
8	H	0.257556	0.28763	44	C	0.009012	-0.06272
9	C	0.009016	-0.05458	45	C	-0.17697	-0.24844
10	C	-0.17697	-0.24863	46	H	0.183214	0.23135
11	H	0.183216	0.22624	47	C	-0.18242	-0.21721
12	C	-0.18242	-0.22399	48	H	0.188746	0.24536
13	H	0.188747	0.24454	49	C	-0.18403	-0.23838
14	C	-0.18403	-0.23783	50	H	0.190087	0.24446
15	H	0.190088	0.24366	51	C	-0.18176	-0.226
16	C	-0.18176	-0.22341	52	H	0.191285	0.24465
17	H	0.191285	0.24384	53	C	-0.17602	-0.22458
18	C	-0.17602	-0.2277	54	H	0.192236	0.24129
19	H	0.192234	0.24245	55	C	-0.36979	-0.3656
20	C	-0.36981	-0.35085	56	C	0.37293	0.22568
21	C	0.372934	0.2238	57	C	-0.59781	-0.70643
22	C	-0.59782	-0.70653	58	H	0.242664	0.24544
23	H	0.242663	0.2453	59	H	0.197974	0.227
24	H	0.197976	0.22637	60	H	0.246672	0.26099
25	H	0.246675	0.26247	61	C	-0.03467	-0.06863
26	C	-0.03467	-0.06978	62	C	-0.21812	-0.10338
27	C	-0.21812	-0.09712	63	H	0.243342	0.12813
28	H	0.243337	0.12819	64	C	-0.17587	-0.21638
29	C	-0.17587	-0.19096	65	H	0.218091	-0.184
30	H	0.21809	-0.18743	66	C	-0.19307	-0.23435
31	C	-0.19307	-0.23478	67	H	0.197867	0.22665
32	H	0.19787	0.22787	68	C	-0.18269	-0.24134
33	C	-0.18268	-0.24223	69	H	0.195581	0.24506
34	H	0.195581	0.24623	70	C	-0.19438	-0.20181
35	C	-0.19438	-0.19899	71	H	0.189295	0.23989
36	H	0.189295	0.24049				

free ligand. The complex binds the 1BNA to the major grove instead of the minor grove position (Fig. 9c) [44, 45]. Only one hydrogen bond *via* sulfur of dithioate and adenine (DA18:H62) with 2.234 Å length has been detected (Fig. 9d); moreover, a lower binding energy of -6.34 kcal/mol has been recorded as seen in Table 4. Additionally, inhibition constant (IC) value of *cis*-Ni(PPEHCDT)$_2$ complex is lower than that of the free ligand which reflects the complex as better 1BNA binder (Table 4). However, they usually used the binding energy values in the final judgment on the ability of compounds to bind with DNA better, since it is a more reliable parameter. Conversely, the ligand efficiency values aligned with the bonding energy values, indicating that the free PPEHCDT ligand is a more effective DNA-binder compared to its *cis*-Ni(PPEHCDT)$_2$ complex, as PPEHCDT exhibited a higher negative B.E value (Table 4).

Conclusions

A novel neutral Nickel(II) complex with two Ni(PPEHDC)$_2$ bidentate N, S-type ligands has been prepared in a good yield. The structural formula of *cis*-Ni(PPEHDC)$_2$ isomer was evidenced by XRD and further supported *via* EDX, IR, UV-Vis, CHN-EA, and FAB-MS analysis. X-ray diffraction reflected the *cis*-Ni(PPEHDC)$_2$ complex with distorted square planar as opposed to the tetrahedral geometry revealed by the DFT theoretical analysis. The *cis*-Ni(PPEHDC)$_2$ was chelated to the Ni(II) center *via* S-thiol and N-azomethine atoms to form a unique cis-conformation square planar. Additionally, the DFT/XRD angles

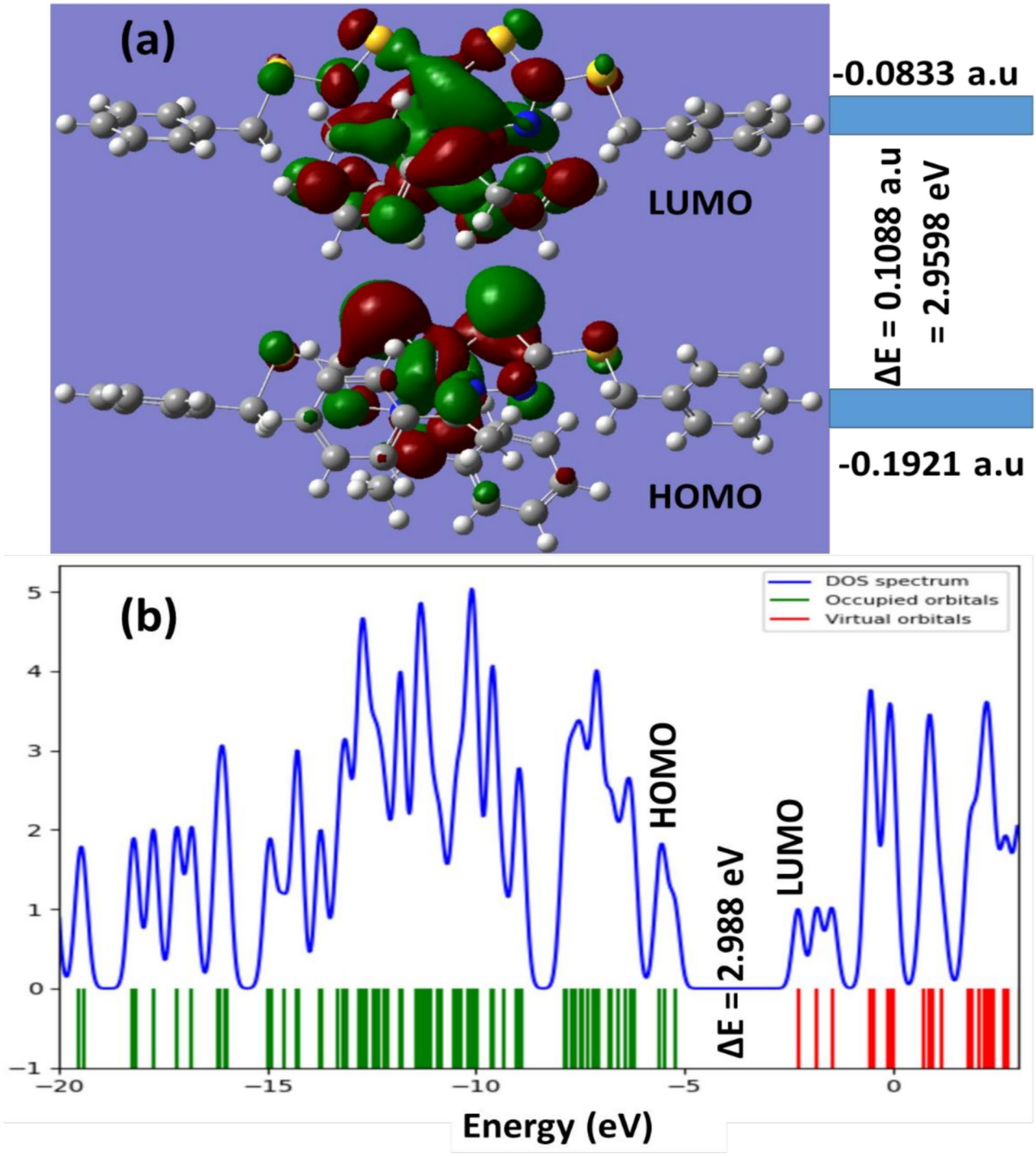

Fig. 7 (**a**) HOMO and LUMO shapes and energy and (**b**) DOS diagrams of *cis*-Ni(PPEHDC)$_2$ complex

and bond length values were of good consistency. The MEP, MAC/NPA, and HSA calculation results proved the XRD-experimental result in the 2D-S24 synthons formation via C-H···πPh and C-H···S interactions. The *cis*-Ni(PPEHDC)$_2$ is thermally stable up to 250 ºC; it decomposed to nickel oxide final product in a two-step decomposition mechanism. Moreover, investigations of 1BNA docking with the free ligand and its Ni-complex showed a dramatical shift in binding locations, H-bond quantity and type, and binding energy values.

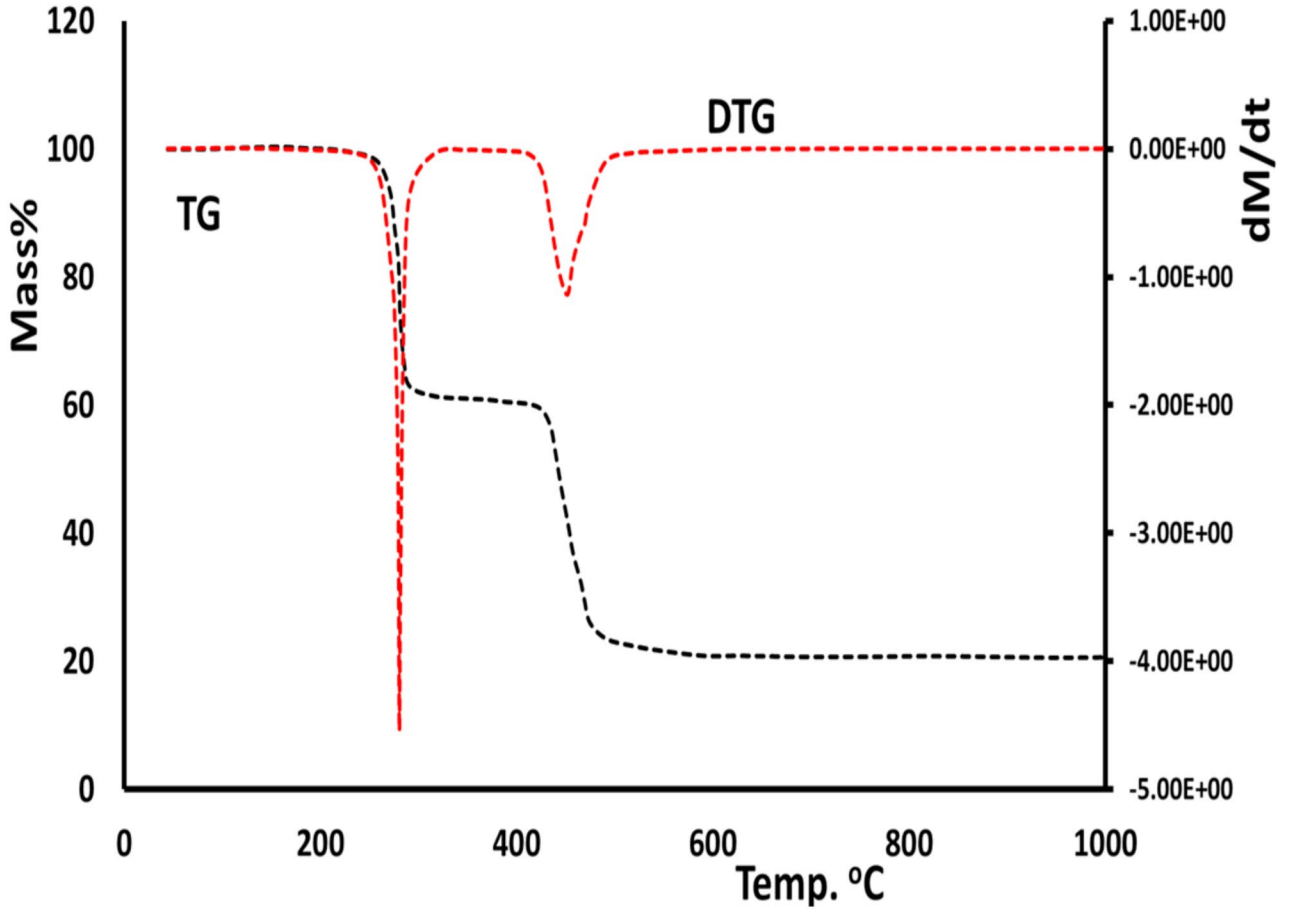

Fig. 8 TGA of the *cis*-Ni(PPEHDC)$_2$ complex

Table 4 Docking data of both the PPEHCDT and its *cis*-Ni(PPEHCDT)$_2$

No.	B.E (kcal/mol)	Ligand Efficiency	I. C, μM T = 298. 15 K	Hb of residues and ligands with bond length (Å)
PPEHDC	-8.84	-0.47	9.78	DNA: B:DC23:O4….H (1.985) DNA: A:DG4:H22….S (2.323)
cis-Ni(PPEHDC)$_2$	-6.34	-0.11	1.35	DNA: B:DA18:H62….S (2.234)

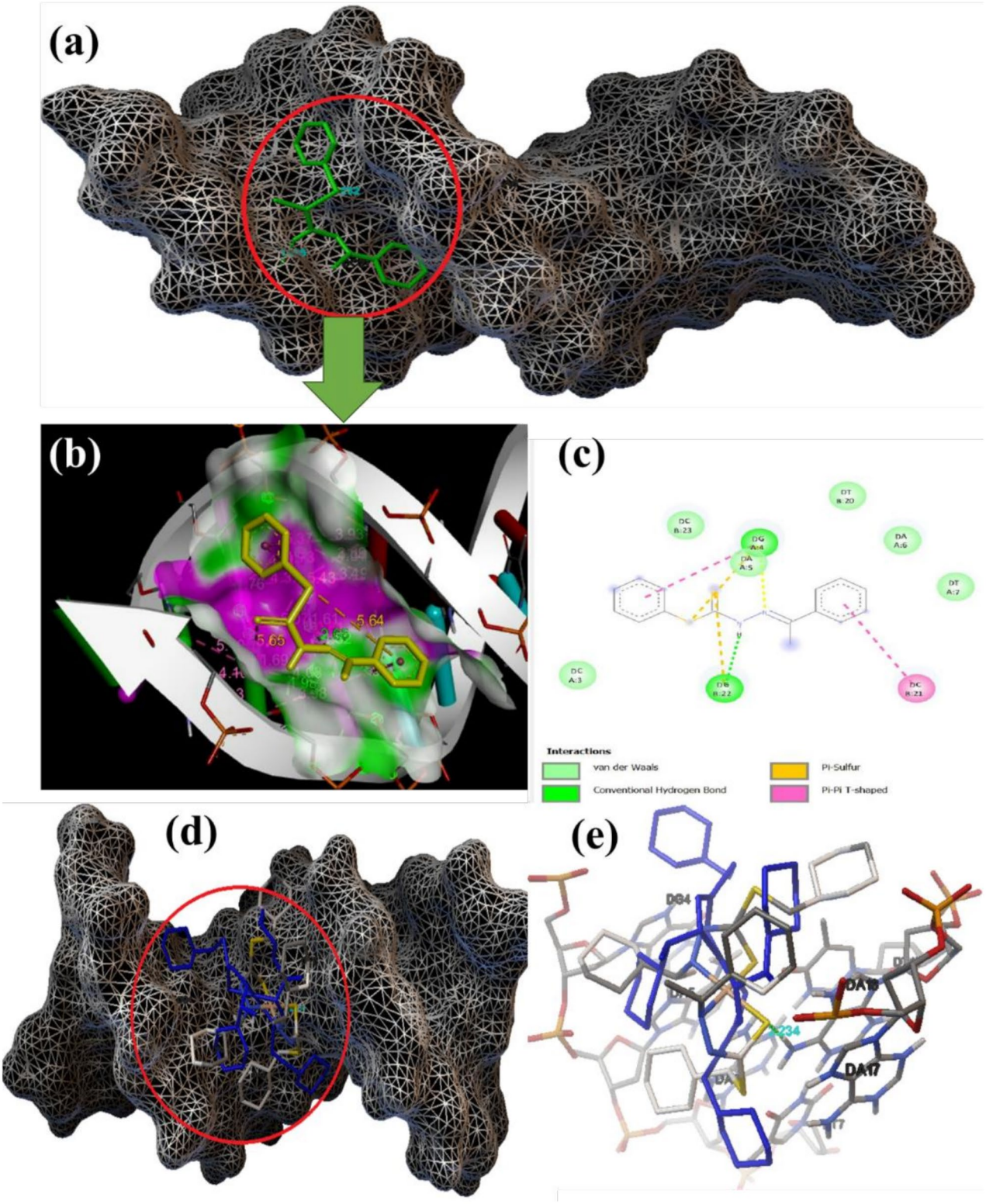

Fig. 9 Docking result of both the PPEHCDT and its *cis*-Ni(PPEHCT)$_2$ with 1BNA: (**a**) PPEHCDT 's connection site, (**b**) 2D-interactions of PPEHCDT, (**c**) *cis*-Ni(PPEHCDT)$_2$'s connection site, and (**d**) Nucleotides medium with their H-bond interacted to *cis*-Ni(PPEHCDT)$_2$

Acknowledgements
The authors extend their sincere thanks to Dr. Ulrich Florke, Department Chemie, Universität Paderborn, Warbuger Strasse 100, 33098 Paderborn, Germany for free solving of the crystal structure. Similar thanks go to Prof. Faisal Abdul Azim Al-Abdali, the General Manger of the Libyan Authority for Scientific Research for his unlimited support; special thanks go to staff members at the Libyan Authority for Scientific Research and Manchester Salt and Catalysis Ltd, UK. Other thank go to Dr. Aysha Mezoughi Tripoli University chemistry department for providing chemicals and lab facilitates.

Author contributions
Author Contributions: Study concept and design (A.B., I.W.); data acquisition (A.F.A., I.M.); methodology (R.A., I.K., N.G.), software (I.W., A.Z.); analysis and interpretation of data (I.W., A.B., N.A.M.); drafting of the manuscript (A.B., I.W., K.S.); critical revision of the manuscript (I.W., N.A.M., H.Q.), supervision (A.B., I.W.).

Funding
This study did not receive any external support.

Data availability
The datasets used and/or analyzed during the current study are available from the corresponding author on reasonable request.

Declarations

Ethics approval and consent to participate
Not applicable.

Consent for publication
Not applicable.

Competing interests
The authors declare no competing interests.

Author details
[1]Libyan Authority for Scientific Research, Tripoli, Libya
[2]School of Chemistry, Biomedical Sciences Research Complex, University of St Andrews, North Haugh, St Andrews, Fife KY16 9ST, UK
[3]Department of Applied Chemistry, Arab American University (AAUP), JeninP.O Box 240, Palestine
[4]Biochemistry Department, Benghazi University, Benghazi, Libya
[5]Department of Applied Medical Science, Libyan International Medical University, Benghazi, Libya
[6]Department of Chemistry Faculty of Science, University of Tripoli, Tripoli, Libya
[7]Libyan Advanced Centre for Chemical analysis, Tajour, Libya
[8]Laboratory of Materials, Nanotechnology and Environment, Faculty of Sciences, Mohammed V University in Rabat, P.O. Box. 1014, Rabat, Morocco
[9]Department of Dentistry and Dental Surgery, Faculty of Medicine and Health Sciences, An-Najah National University, P.O. Box 7, Nablus, Palestine
[10]Department of Chemistry, Science College, An-Najah National University, P.O. Box 7, Nablus, Palestine

Received: 27 January 2024 / Accepted: 2 April 2025
Published online: 22 April 2025

References

1. Boshaala A, Salih KSM, Bader N, Almughery AA, Zarrouk A, Warad I. XRD/HSA, noncovalent interactions and influence of solvent Polarity on spectral properties of dithiocarbazate schiff base and its cis-Cu(II) complex: experimental and theoretical studies. J Mol Liq. 2021;330:115551.
2. Singh NK, Bharty MK, Kushawaha SK, Singh UP. Pooja Tyagi, synthesis, spectral and structural studies of a Mn(II) complex of [N′-(pyridine-4-carbonyl)-hydrazine]-carbodithioic acid Ethyl ester and Mn(II) and Ni(II) complexes of [N′-(pyridine-4-carbonyl)-hydrazine]-carbodithioic acid Methyl ester. Polyhedron. 2010;29:1902.
3. Otero L, Vieites M, Boiani L, Denicola A, Rigol C, Opazo L, Olea-Azar C, Maya JD, Morello A, Krauth-Siegel RL, Piro OE, Castellano E, Gonzalez M, Gambino D, Cerecetto H. Novel antitrypanosomal agents based on palladium nitrofurylthiosemicarbazone complexes: DNA and redox metabolism as potential therapeutic targets. J Med Chem. 2006;49:3322.
4. Tarafder MTH, Ali MA, Wee DJ, Azahari K, Silong S, Crouse DA. Coordination chemistry and biological activity of nickel (II) and copper(II) ion complexes with nitrogen–sulphur donor ligands derived from S-benzyldithiocarbazate (SBDTC). Trans Met Chem. 2000;25:456.
5. Beckett R, Hoskins BF. Square-planar complexes of pentane-2, 4-dithione (dithioacetylacetone): crystal structures of the Cobalt (II) and nickel (II) derivatives. J Chem Soc Dalton Trans (1974) 622.
6. Singh V, Chauhan R, Kumar A, Bahadur L, Singh N. Efficient phenylmercury (II) Methylferrocenyldithiocarbamate functionalized dye-sensitized solar cells. Dalton Trans. 2010;39:9779.
7. eizi HF, Shiri F, Bagheri R, Singh J, Chae KH, Song Z, Najafpour MM. The application of a nickel(ii) schiff base complex in water oxidation: the importance of nanosized materials. Catal Sci Technol. 2018;8:3954.
8. Najafpour MM, Renger G, Hołyn´ ska M, Moghaddam AN, Aro E-M, Carpentier R, Nishihara H, Eaton-Rye JJ, Shen J-R, Allakhverdiev SI. Nanosized manganese oxide/holmium oxide: A new composite for water oxidation. Chem Rev. 2016;116:2886.
9. Rüttinger W, Dismukes GC. Synthetic water-oxidation catalysts for artificial photosynthetic water oxidation. Chem Rev. 1997;97:1.
10. McEvoy JP, Brudvig GW. Water-splitting chemistry of photosystem II. Chem Rev. 2006;106:4455.
11. Sarkar S, Nag SK, Chattopadhyay AP, Dey K, Islam SM, Sarkar A, Sarkar S. Synthesis, structure and catalytic activities of nickel(II) complexes bearing N4 tetradentate schiff base ligand. J Mol Struct. 2018;1160:9.
12. Cao Y, Lu M, Fang J, Shi L, Zhang D. Hexagonal Boron nitride supported mesosio 2-confined Ni catalysts for dry reforming of methane. Chem Commun. 2017;53:7549.
13. Han Y, Wu Y, Lai W, Cao R. Electrocatalytic water oxidation by a water-Soluble nickel porphyrin complex at neutral pH with low overpotential. Inorg Chem. 2015;54:5604.
14. Najafpour MM, Feizi H. Nano-sized manganese oxide: a proposed catalyst for water oxidation in the reaction of some manganese complexes and cerium (IV) ammonium nitrate. Dalton Trans. 2012;41:10292.
15. Schley ND, Blakemore JD, Subbaiyan NK, Incarvito CD, D'Souza F, Crabtree RH, Brudvig GW. Elucidating molecular iridium water oxidation catalysts using Metal–Organic frameworks: A comprehensive structural, catalytic, spectroscopic, and kinetic study. J Am Chem Soc. 2011;133:10473.
16. Zhang M, Zhang MT, Hou C, Ke ZF, Lu TB. Angew. Homogeneous electrocatalytic water oxidation at neutral pH by a robust macrocyclic nickel (II) complex chem. Int Ed. 2014;53:13042.
17. Grivani G, Khalaji AD, Tahmasebi V, Gotoh K, Ishida H. Synthesis, characterization and crystal structures of new bidentate schiff base ligand and its vanadium(IV) complex: the catalytic activity of Vanadyl complex in epoxidation of alkenes. Polyhedron. 2012;31:265.
18. Lippard SJ, Berg JM. Principles of bioinorganic chemistry. California: University Science Books; 1994.
19. Amini M, Arab A, Soleyman R, Ellern A, Woo LK. Synthesis, characterization and crystal structures of oxovanadium(V) complexes derived from similar aroylhydrazone ligands. J Coord Chem. 2013;66:3770.
20. Khadir N, Amini M, Assoud A, Bagherzadeh M, Boghaei DM. Synthesis and characterization of two binuclear nickel(II) complexes of thiophenol-based end-off compartmental ligands and their application as catalysts for selective oxidation of sulfides. J Coord Chem. 2016;69:103.
21. Doukov TI, Iverson TM, Seravalli J, Ragsdale SW, Drennan CL. A Ni-Fe-Cu center in a bifunctional carbon monoxide dehydrogenase/ Acetyl-CoA synthase. Science. 2002;298:567.
22. Wuerges J, Lee JW, Yim YI, Yim HS, Kang SO, Carugo KD. Crystal structure of nickel-containing superoxide dismutase reveals another type of active site. Proc Natl Acad Sci USA. 2004;101:8569.
23. Boshaala A, Yamin BM, Ben Amer YO, Ghaith GSH, Almughery AA, Zarrouk A, Warad I. Crystal interaction, Hirshfeld surface analysis, and spectral analysis of new dithiocarbazate schiff bases derivative (LH) and its neutral cis-Cu (L) 2 complex. J Mol Struct. 2021;1224:129207.
24. Boshaala AM, AlFarha KA, Sheppaek H, Algezzeri WO, Zarrouk A, Warad I. Crystal interaction, XRD powder, and Hirshfeld surface analysis of S-benzyl-β-N-(1-(4-chlorophenyl) ethylidene) dithiocarbazate schiff base. Mor J Chem. 2020;8:1048.

25. Lindner E, Warad I, Eichele K, Mayer HA. Supported organometallic complexes part 34: synthesis and structures of an array of diamine(ether-phosphine) ruthenium(II) complexes and their application in the catalytic hydrogenation of trans-4-phenyl-3-butene-2-one. Inorg Chim Acta. 2003;350:49.
26. Wolff SK, Grimwood DJ, McKinnon JJ, Turner MJ, Jayatilaka D, Spackman MA. Crystal explorer 3.0. Perth, Australia: University of Western; 2012.
27. Frisch GWTMJ, Schlegel HB, Scuseria GE, Robb MA, Cheeseman JR. Gaussian 09, Revision E.01, Gaussian, Inc., Wallingford CT, 2009.
28. Forli S, Huey R, Pique ME, Sanner MF, Goodsell DS, Olson AJ. Computational protein-ligand Docking and virtual drug screening with the AutoDock suite. Nat Protoc. 2016;11:905.
29. https://www.rcsb.org/structure/1BNA
30. Drew R, Wing M, Takano T, Broka C, Tanaka S, Itakura K, Dickerson E. Proc Natl Acad Sci. 1981;78:2179.
31. Burla M, Caliandro R, Camalli M, Carrozzini B, Cascarano GL, DeCaro L, Giacovazzo C, Polidori G. Spagna SIR2004: an improved tool for crystal structure determination and refinement. J Appl Crystallogr. 2005;38:381.
32. Sheldrich GM. SHELX-97, release 97-2. Germany: University of Goettingen; 1998.
33. Srijana PJ, Narayana B, Sarojini BK, Ai Wong Q, K.Quah C, Likhitha U. Synthesis and structural studies on the supramolecular architecture of two novel proton transfer molecular salts of 2– aminopyridine. J Mol Struct. 2023;1274:134426.
34. Guerraoui A, Djedouani A, Jeanneau E, Boumaza A, Alsalme A, Zarrouk A, Salih KSM, Warad I. Crystal structure and spectral of new hydrazine-pyrandione derivative: DFT enol↔hydrazone tautomerization *via* zwitterionic intermediate, Hirshfeld analysis and optical activity studies. J Mol Struct. 2020;1220:1890.
35. Tabti S, Djedouani A, Aggoun D, Warad I, Rahmouni S, Romdhane S, Fouzi H. New Cu(II), Co(II) and Ni(II) complexes of chalcone derivatives: synthesis, X-ray crystal structure, electrochemical properties and DFT computational studies. J Mol Struct. 2018;1155:11.
36. Hema MK, Karthik CS, Warad I, Lokanath NK, Zarrouk A, Kumara K, Pampa KJ, Mallu P. Regular square Planer bis-(4,4,4-trifluoro-1-(thiophen-2-yl)butane1,3-dione)/copper(II) complex: *Trans/cis*-DFT isomerization, crystal structure, thermal, solvatochromism, Hirshfeld surface and DNA binding analysis. J Mol Struct. 2018;1157:69.
37. Spackman MA, Jayatilaka D. Hirshfeld Surf Anal CrystEngComm. 2009;11:19.
38. Warad I, Awwadi FF, Abd Al-Ghani B, Sawafta A, Shivalingegowda N, Lokanath NK, Mubarak MS, Ben Hadda T, Zarrouk A, Al-Rimawi F, Odeh AB, Barghouthi SA. Ultrasound-assisted synthesis of two novel [CuBr(diamine)$_2$H$_2$O]Br complexes: solvatochromism, crystal structure, physicochemical, Hirshfeld surface thermal, DNA/binding, antitumor and antibacterial activities. Ultrason Sonochem. 2018;48:1.
39. Hema MK, Karthik CS, Lokanath NK, Mallu P, Zarrouk A, Salih KSM, Warad I. Synthesis of novel Cubane [Ni$_4$(O∩O)$_4$(OCH$_3$)$_4$(OOH)$_4$] cluster: XRD/HSA-interactions, spectral, DNA-binding, Docking and subsequent thermolysis to NiO nanocrystals. J Mol Liq. 2020;315:113756.
40. Aouad MR, Messali M, Rezki N, Said MA, Lentz D, Zubaydi L, Warad I. Hydrophobic pocket docking, double-proton prototropic tautomerism in contradiction to single-proton transfer in thione⇔ thiol schiff base with triazole-thione moiety: green synthesis, XRD and DFT-analysis. J Mol Struct. 2019;1180:455.
41. Aouad MR, Messali M, Rezki N, Al-Zaqri N, Warad I. Single proton intramigration in novel 4-phenyl-3-((4-phenyl-1H-1,2,3-triazol-1-yl)methyl)-1H-1,2,4-triazole-5(4H)-thione: XRD-crystal interactions, physicochemical, thermal, Hirshfeld surface, DFT realization of Thiol/thione tautomerism. J Mol Liq. 2018;264:621.
42. Faydy ME, About H, Warad I, Kerroum Y, Berisha A, Podvorica F, Bentiss F, Kaichouh G, Lakhrissi B, Zarrouk A. Insight into the corrosion Inhibition of new bis-quinolin-8-ols derivatives as highly efficient inhibitors for C35E steel in 0.5 M H_2SO_4. J Mol Liq. 2021;342:117333.
43. Ray B, Mehrotra R. Nucleic acid binding mechanism of flavone derivative: structural analysis to unveil anticancer potential. J Photochem Photobiol B: Biol. 2020;211:111990.
44. Haleel AK, Mahendiran D, Rafi UM, Veena V, Shobana S. Rahiman Tetrazolo[1,5-a]pyrimidine-based metal(II) complexes as therapeutic agents: DNA interaction, targeting topoisomerase I and cyclin-dependent kinase studies. Inorg Nano-Met Chem. 2018;48:12.
45. Baronea G, Terenzi A, Lauria A, Maria Almerico A, Leal JM, Bustoc N, García B. DNA-binding of nickel(II), copper(II) and zinc(II) complexes: Structure–affinity relationships. Coor Chem Revi. 2013;257:2848.
46. BIOVIA DS. Discover Studio Visualiser v19.10.18287. 2018 (San Diego, USA).

Publisher's note

Terms and Conditions

Springer Nature journal content, brought to you courtesy of Springer Nature Customer Service Center GmbH (“Springer Nature”).
Springer Nature supports a reasonable amount of sharing of research papers by authors, subscribers and authorised users (“Users”), for small-scale personal, non-commercial use provided that all copyright, trade and service marks and other proprietary notices are maintained. By accessing, sharing, receiving or otherwise using the Springer Nature journal content you agree to these terms of use (“Terms”). For these purposes, Springer Nature considers academic use (by researchers and students) to be non-commercial.
These Terms are supplementary and will apply in addition to any applicable website terms and conditions, a relevant site licence or a personal subscription. These Terms will prevail over any conflict or ambiguity with regards to the relevant terms, a site licence or a personal subscription (to the extent of the conflict or ambiguity only). For Creative Commons-licensed articles, the terms of the Creative Commons license used will apply.
We collect and use personal data to provide access to the Springer Nature journal content. We may also use these personal data internally within ResearchGate and Springer Nature and as agreed share it, in an anonymised way, for purposes of tracking, analysis and reporting. We will not otherwise disclose your personal data outside the ResearchGate or the Springer Nature group of companies unless we have your permission as detailed in the Privacy Policy.
While Users may use the Springer Nature journal content for small scale, personal non-commercial use, it is important to note that Users may not:

1. use such content for the purpose of providing other users with access on a regular or large scale basis or as a means to circumvent access control;
2. use such content where to do so would be considered a criminal or statutory offence in any jurisdiction, or gives rise to civil liability, or is otherwise unlawful;
3. falsely or misleadingly imply or suggest endorsement, approval , sponsorship, or association unless explicitly agreed to by Springer Nature in writing;
4. use bots or other automated methods to access the content or redirect messages
5. override any security feature or exclusionary protocol; or
6. share the content in order to create substitute for Springer Nature products or services or a systematic database of Springer Nature journal content.

In line with the restriction against commercial use, Springer Nature does not permit the creation of a product or service that creates revenue, royalties, rent or income from our content or its inclusion as part of a paid for service or for other commercial gain. Springer Nature journal content cannot be used for inter-library loans and librarians may not upload Springer Nature journal content on a large scale into their, or any other, institutional repository.
These terms of use are reviewed regularly and may be amended at any time. Springer Nature is not obligated to publish any information or content on this website and may remove it or features or functionality at our sole discretion, at any time with or without notice. Springer Nature may revoke this licence to you at any time and remove access to any copies of the Springer Nature journal content which have been saved.
To the fullest extent permitted by law, Springer Nature makes no warranties, representations or guarantees to Users, either express or implied with respect to the Springer nature journal content and all parties disclaim and waive any implied warranties or warranties imposed by law, including merchantability or fitness for any particular purpose.
Please note that these rights do not automatically extend to content, data or other material published by Springer Nature that may be licensed from third parties.
If you would like to use or distribute our Springer Nature journal content to a wider audience or on a regular basis or in any other manner not expressly permitted by these Terms, please contact Springer Nature at

onlineservice@springernature.com